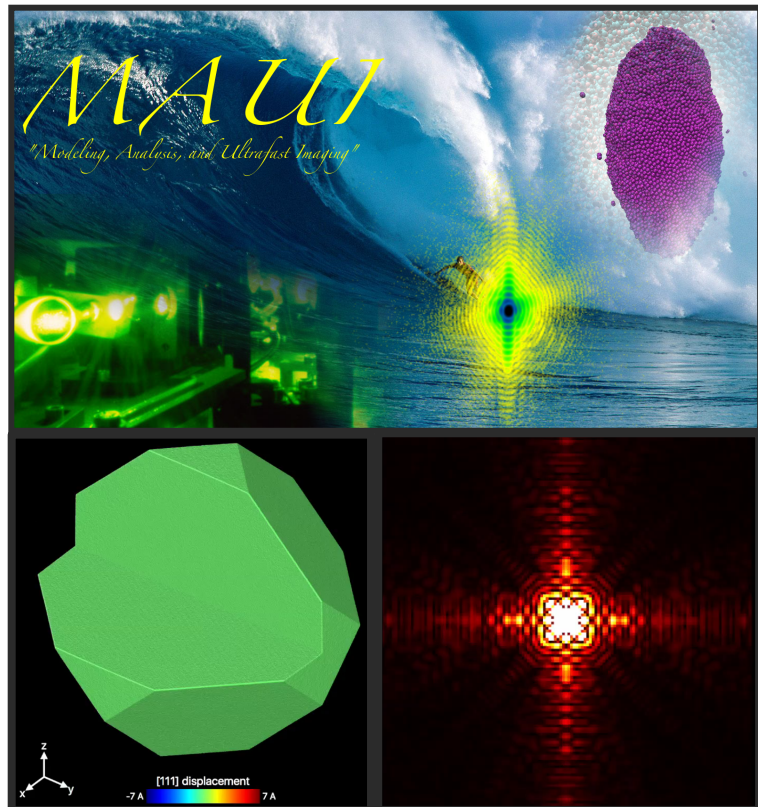


Lattice Dynamics of Core-Shell Bimetallic Nanocrystals during Ultrafast Laser Excitation



Kiran Sasikumar

Postdoctoral Researcher

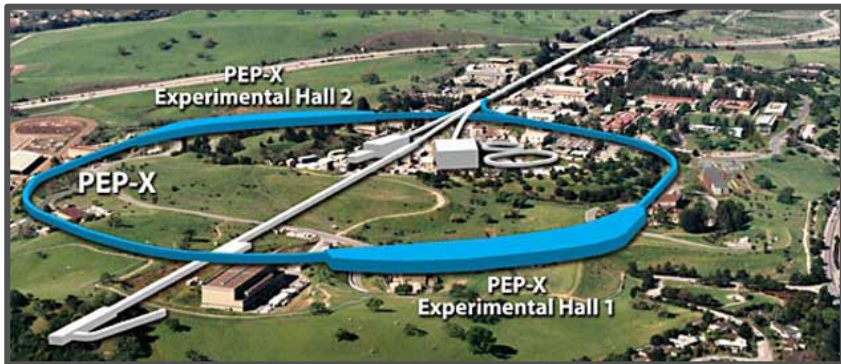
Supervisor: Subramanian Sankaranarayanan

Center for Nanoscale Materials
Nanoscience and Technology Division
Argonne National Laboratory

Authors: K. Sasikumar, M. J. Cherukara, J.
N. Clark, T. Peterka, R. Harder, S.K.R.S.
Sankaranarayanan



ACKNOWLEDGEMENTS



This work is performed as part of the DOE LDRD proposal titled “integrated imaging, modeling, and analysis of ultrafast energy transport in nanomaterials”.

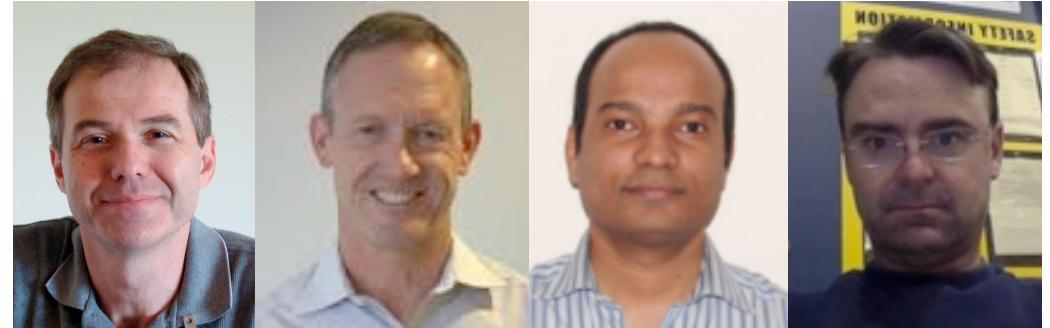
The research utilized resources of the Argonne Leadership Computing Facility, Center for Nanoscale Materials (Carbon computing cluster) and the Advanced Photon Source, a U.S. Department of Energy (D.O.E) Office of Science User Facility operated for the D.O.E Office of Science by Argonne National Laboratory under Contract No. DE-AC02-06CH11357. Experiments were also conducted at the Stanford PULSE Institute, SLAC National Accelerator Laboratory, USA. We thank the staff at Argonne National Laboratory and collaborators at SLAC National Accelerator Laboratory for the experimental samples and data analysis.



ACKNOWLEDGEMENTS

Modeling

- ❖ Subramanian Sankaranarayanan (CNM)
- ❖ Kiran Sasikumar (CNM)



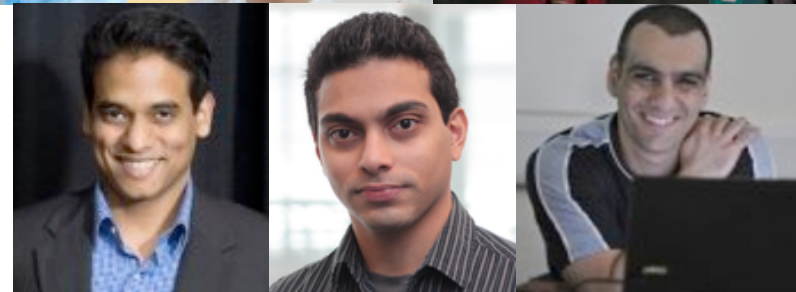
Analysis

- ❖ Todd Munson (MCS)
- ❖ Sven Leyffer (MCS)
- ❖ Nicola Ferrier (MCS)
- ❖ Youssef Nashed (MCS)
- ❖ Tom Peterka (MCS)



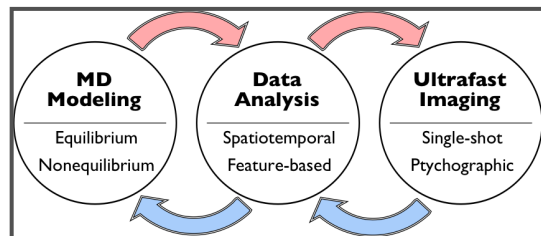
Ultrafast Imaging

- ❖ Ian McNulty (NST)
- ❖ Ross Harder (XSD)
- ❖ Haidan Wen (XSD)
- ❖ Mathew Cherukara (XSD)
- ❖ Andrew Ulvestad (MSD)
- ❖ Jesse Clark (Stanford/SLAC)



Modeling, Analysis and Ultrafast Imaging

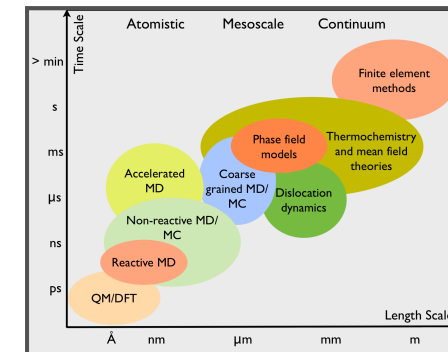
What is MAUI?



Integrating imaging and simulation

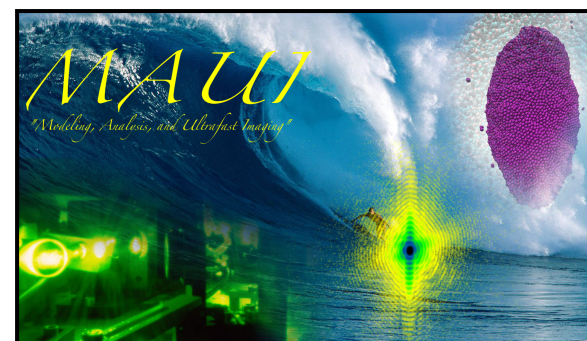
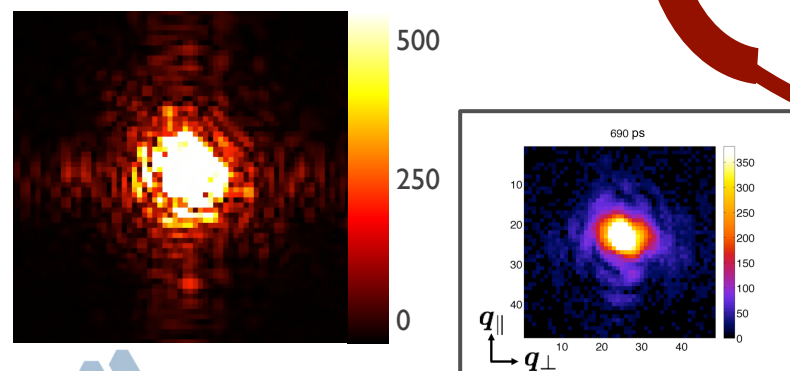
³He), the breaking of symmetry in ³He-A. Chirality is a fundamental property of matter. We report direct detection of chiral domains in the superfluid free surface of ³He-A. In particular, we detected domains by a moving electron; the direct measurement of the chirality showed that, at the superfluid transition, the domains are randomly oriented. The observation of such selected domains provides a clear evidence for the spontaneous symmetry breaking in ³He-A.

J. N. Clark et. al.,
Science 341 (2013).



MAUI IDEAL:

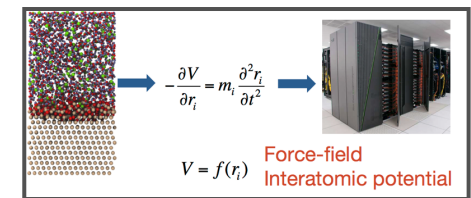
- Simulations complement experiments to reveal new theory.
- Directly compare simulation and experiments to iteratively improve both methodologies.



BCDI measured diffraction pattern vs. simulated

Simulation via molecular dynamics

What is molecular dynamics?



Integrating ultrafast imaging with atomistic simulations to investigate lattice dynamics of core-shell bimetallic nanocrystals during pulsed heating

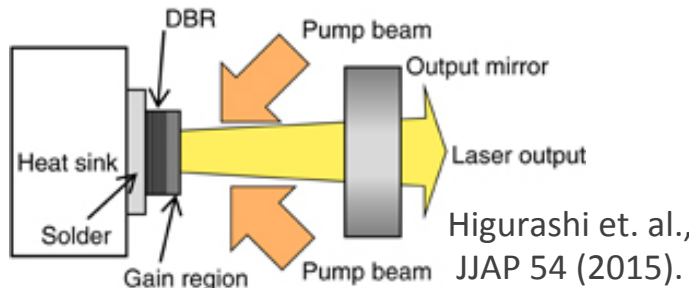
Project Goals:

- ✧ Develop **automated workflow tools** and protocols to integrate experimental BCDI measurements with large-scale molecular dynamics simulations.
- ✧ Demonstrate application of workflow to understand the mechanical and dynamical properties of externally stimulated nanoparticles at femtosecond and picosecond timescales.
 - **Pulsed laser heating of core-shell bimetallic nanocrystals.**



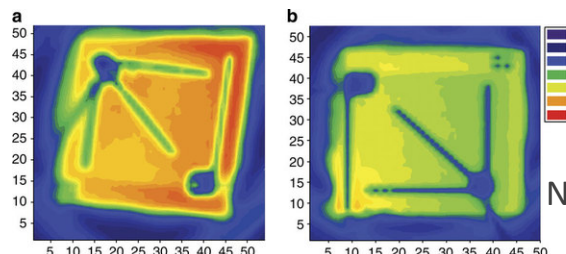
Heat, phonons and lattice vibrations

Several applications where understanding heat dissipation mechanisms are important.



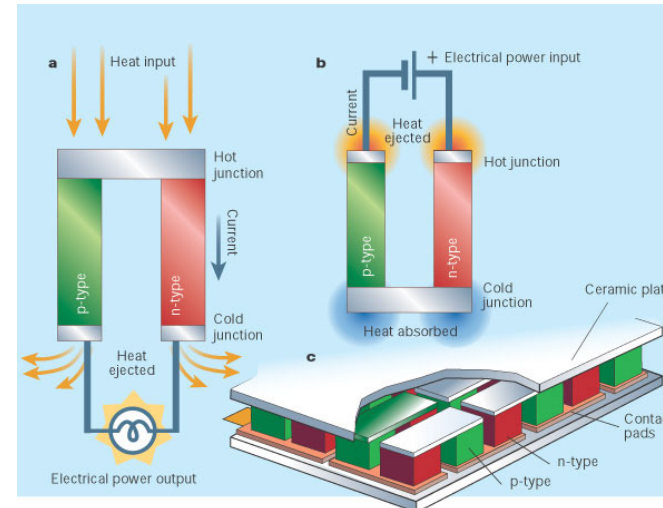
Higurashi et. al.,
JJAP 54 (2015).

Heat dissipation in high-power semiconductor lasers



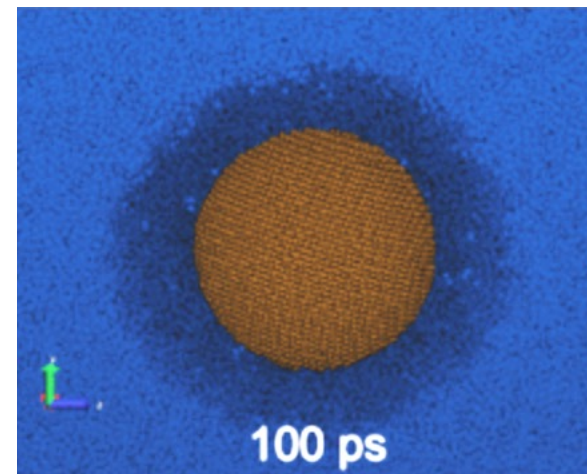
Han et. al.,
Nat. Comm. 4
(2013).

Heat dissipation in gallium nitride light-emitting diodes with embedded graphene oxide pattern



Cronin B. Vining,
Nature 413
(2001).

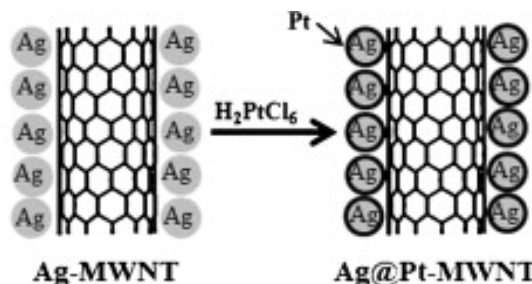
Waste heat energy conversion in thermoelectrics



Nanoscale cavitation in intensely heated nanofluids for biomedical applications

Sasikumar et. al.,
J. Chem. Phys.
141 (2014).

Core-shell nanoparticles



Rashid et. al., Sensors and Actuators B: Chemical Vol. 208 (2015).

Bimetallic core–shell Ag@Pt nanoparticle-decorated MWNT electrodes for H₂ sensors and direct methanol fuel cells

particle size, with a complete interdiffusion at room temperature for core sizes below 4.6 nm.

These results suggest that the synthesis of well-defined Ag@Au core–shell nanoparticles requires a tight control of the electrochemical potentials and reduction conditions and can only be trusted after careful space-resolved analysis of the metal distribution within the particles.

Gold Nanorod Alignment and Patterning

One of the most exciting properties of anisotropic metal nanoparticles is their polarization dependent response to incident

- (65) Sinzig, J.; Quinten, M. *Appl. Phys. A* **1994**, *58*, 157.
(66) Hodak, J. H.; Henglein, A.; Giersig, M.; Hartland, G. V. *J. Phys. Chem. B* **2000**, *104*, 11708.
(67) Abid, J.-P.; Girault, H. H.; Brevet, P. F. *Chem. Commun.* **2001**, 829.

Liz-Marzan et. al., Langmuir 22 (2006).

Tailoring surface plasmons through the morphology and assembly of metal nanoparticles



Gangopadhyay et. al., IEEE Transactions On Magnetics 41 (2005).

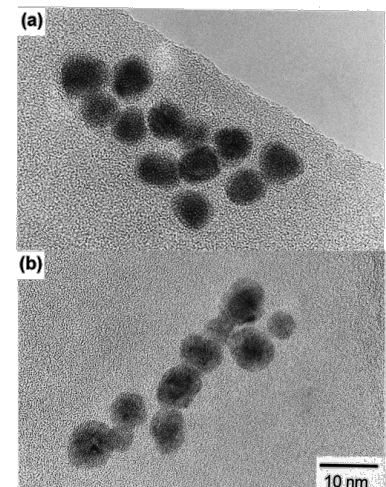
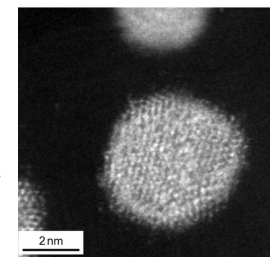
Zhong et. al., Advanced Materials 13 (2001).

Scheme 1. Schematic illustrations of catalytic re-nanoparticle catalyst, and b) at core–shell nanop-

1508

© WILEY-VCH Verlag GmbH,

Strasser et. al., Nature Chemistry 2 (2010).



Mizukoshi et. al., Journal of Physical Chemistry B 104 (2000).

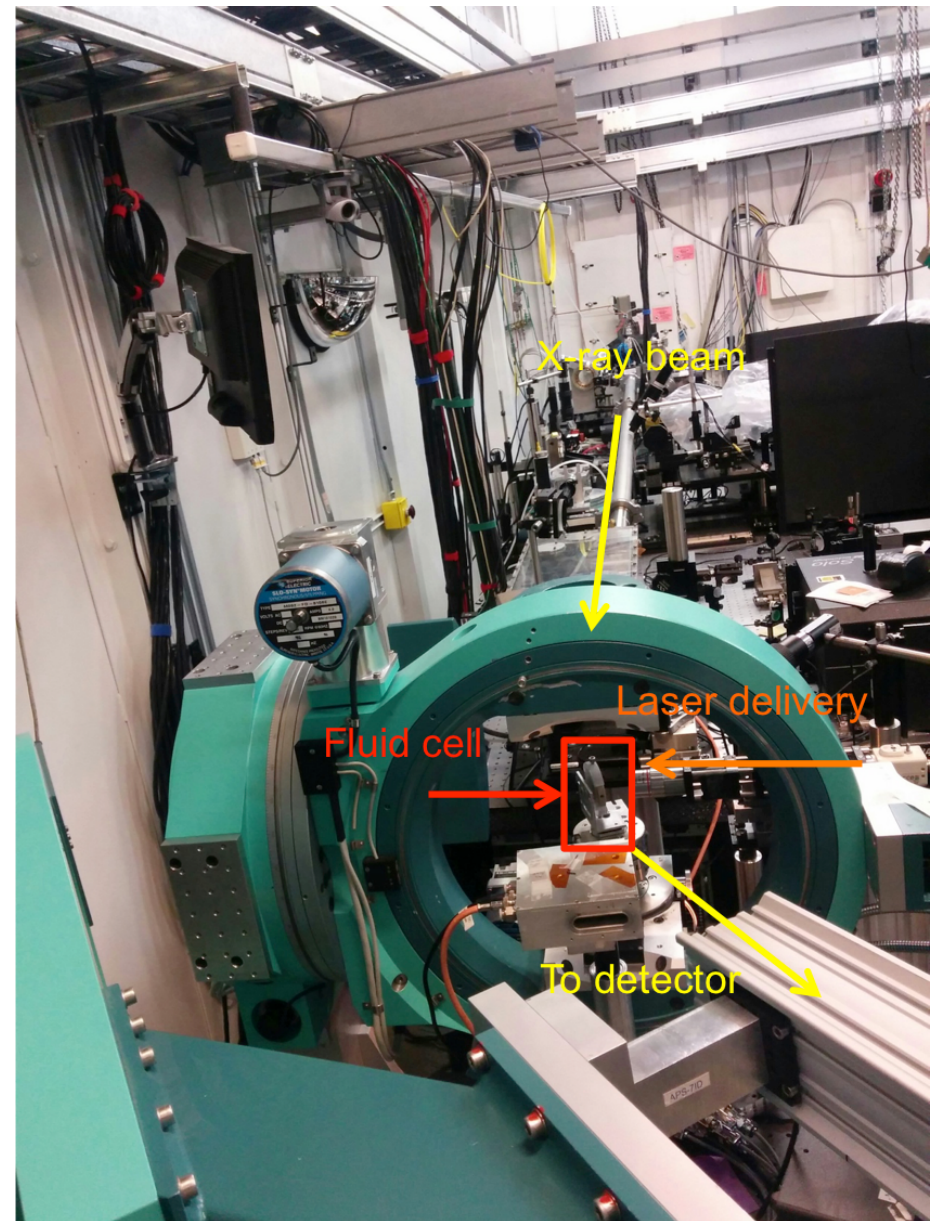
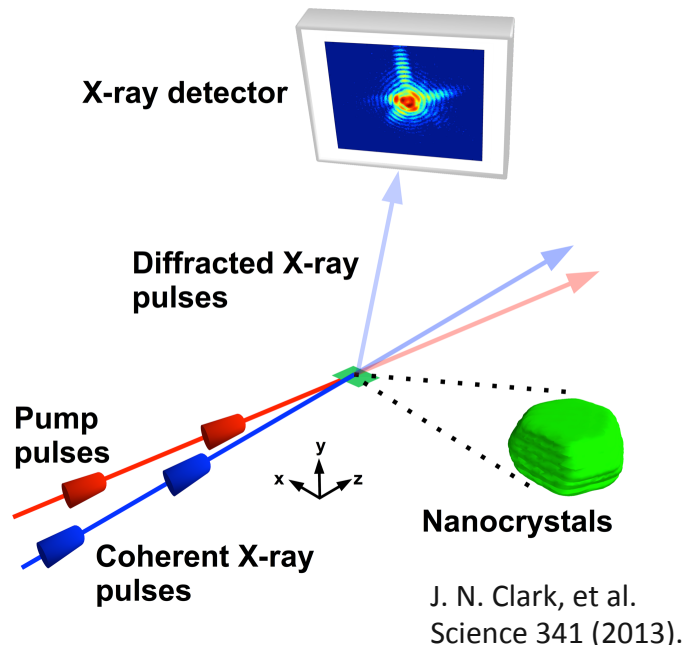
Core-shell nanoclusters for catalysis

dissolved in 50 mL of DMF is added to this solution over a period of 5 min. The solution turns blue and after 10 min stirring, the reaction mixture is cooled and poured into 25 mL of acetone. A dark-colored precipitate is collected over a home-made magnetic filtration system. The solid, thus isolated, is redispersed in water. A few cycles of redispersion, precipitation with acetone, and collection over a magnet ensure isolation. 0.25 g of pure γ -Fe₂O₃(Au) core(shell) nanoparticles of 10 nm diameter are dissolved in 10 mL of water. 0.05 g of bovine serum albumins, 0.1 g of the core(shell) particles is dissolved in 10 mL of Ringer's buffer at pH 7.4 by sonication. Human serum albumin (HSA, 0.1 g) dissolved in 50 mL of Ringer's t-

Superparamagnetic core(shell) nanoparticles for magnetic targeted drug delivery and hyperthermia treatment

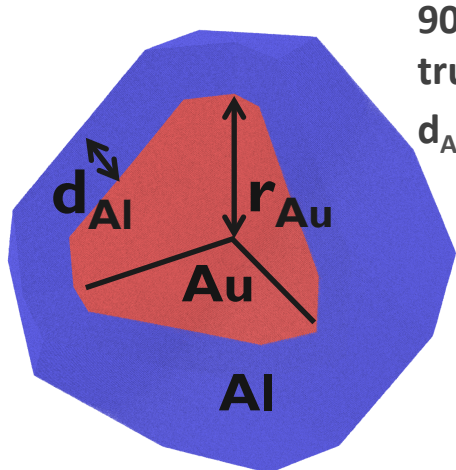
Ultrafast time resolved BCDI

- ❖ Laser pump, X-ray probe.
- ❖ Combine with BCDI.
- ❖ Provide dynamical map of excited modes in sample.
- ❖ <10 nm spatial resolution possible with ps-scale temporal resolution.



The BCDI setup at Argonne's APS.

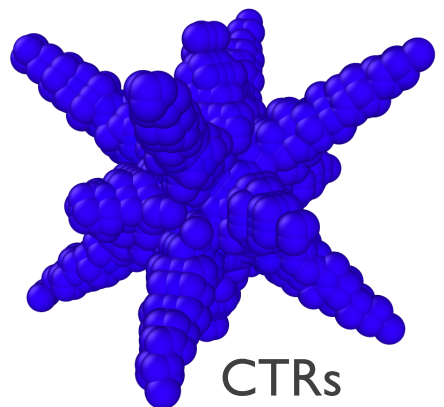
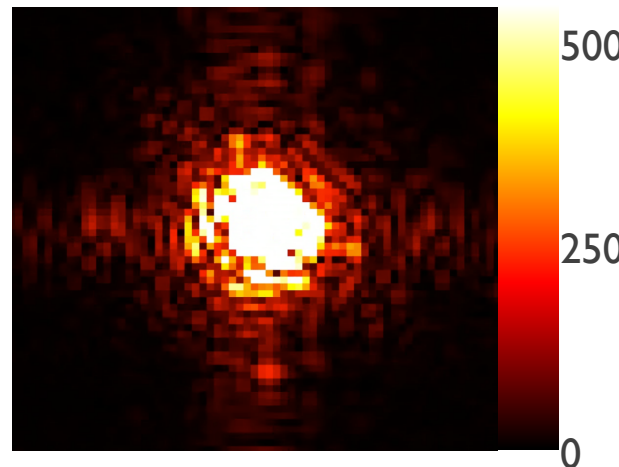
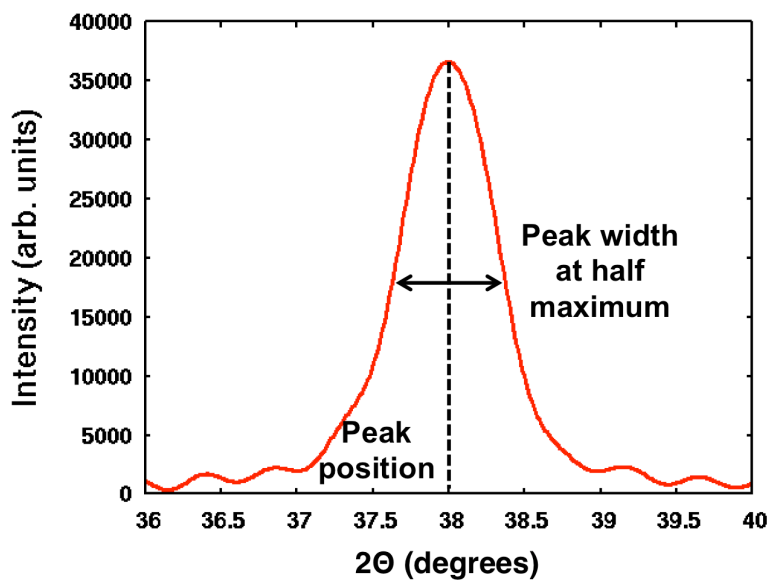
Molecular dynamics



90 nm Au-Al core-shell
truncated octahedron
 $d_{Al}/r_{Au} = 0.3$

$$-\frac{\partial V}{\partial r_i} = m_i \frac{\partial^2 r_i}{\partial t^2}$$

$V = f(r_i) \rightarrow$ Force-field
Interatomic potential (EAM)



Diffraction patterns can be computed from MD trajectories.



Past work: Lattice breathing in gold

J. N. Clark, et al.
Science 341 (2013).

the lifetime of the oscillations is relatively long in comparison to previous studies, because there is no ensemble averaging of heterogeneous periods in our experiment (13–15, 21).

Thus far, we have identified two clear vibration modes in the expansion of the crystal. Further modes, such as shear modes, can be identified only by imaging the crystal distortions directly because these do not result in a shift of the Bragg peak position. Three-dimensional (3D) images as a function of delay time were obtained for nanocrystal I by collecting 3D coherent dif-

in the displacement of the crystal, projected onto the diffraction vector \mathbf{Q} , whose direction is also shown in Fig. 3. The homogeneous (linear) lattice expansion and contraction resulting from the breathing modes of the nanocrystal have been removed (21), leaving only the inhomogeneous component that would manifest itself as a broadening or distortion of the Bragg peak rather than a peak shift. To emphasize the changes, we have subtracted the image at –40 ps from the subsequent times, which removes the contribution of small, static residual stresses in the nanocrystal.

and a height of 220 nm (21). The good agreement between the data, theory, and MD simulation (fig. S2) strongly supports the presence of this otherwise invisible higher-order mode. Observation of this 50-ps amplitude modulation and the presence of a 600-ps breathing mode show considerable sensitivity gain by BCDI in

The combination of intense, coherent, ultrashort x-ray pulses provided by XFELs enabled direct, unambiguous imaging of collective acoustic phonons in gold nanocrystals in three dimensions. The technique demonstrated here

58

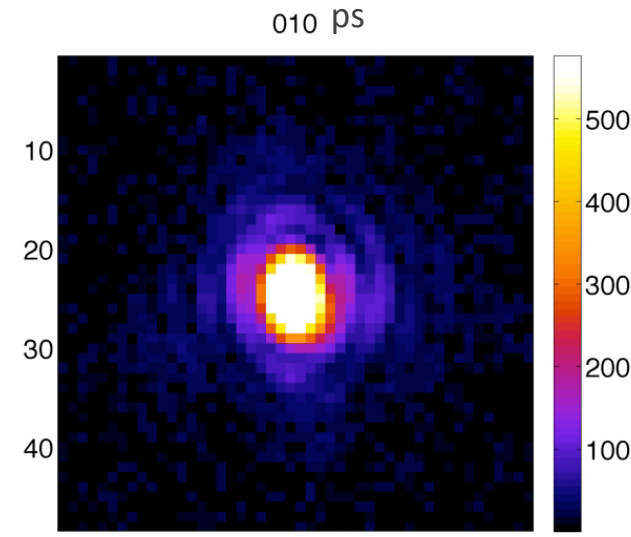
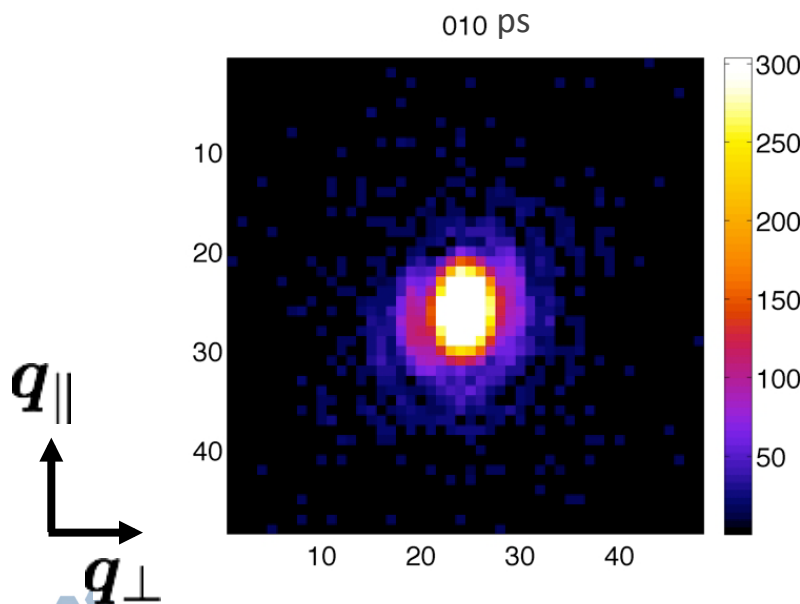
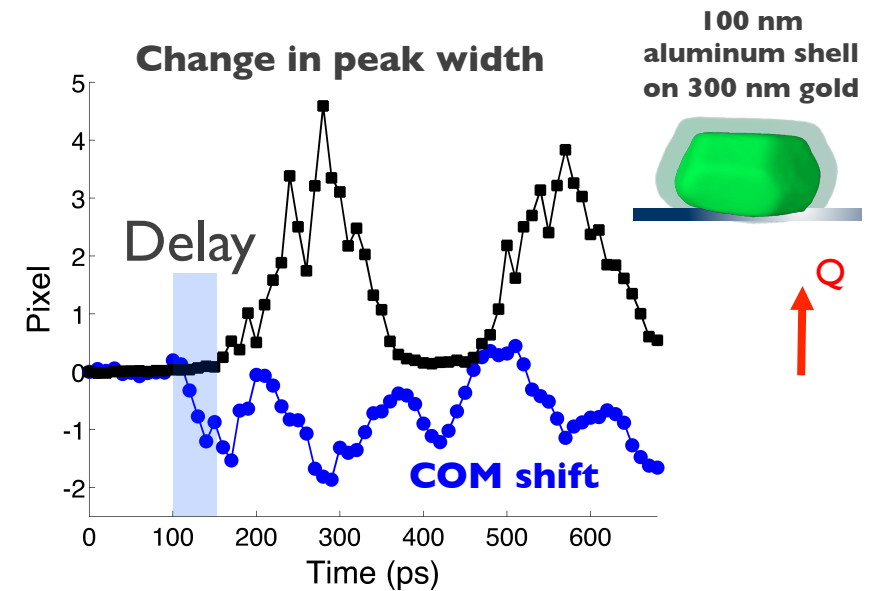
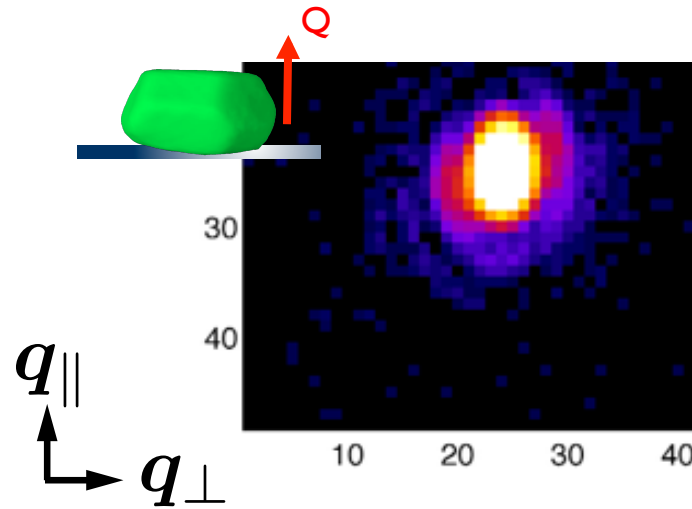
Nanocrystals I and 2

5 JULY 2013 VOL 341 SCIENCE www.sciencemag.org

- ❖ Experimental data for two different nanocrystal sizes.
 - ❖ Observed lattice breathing can be described by 2 modes.
 - Nanocrystal I: 101 and 241 ps.
 - Nanocrystal 2: 90 and 256 ps.
 - ❖ Comparison between experiment and a scaled MD simulation.
 - ❖ MD simulation system sizes ~9 times smaller than experiment.
 - ❖ Homogeneous breathing mode time period can be directly correlated with size.
 - ❖ Related to time taken by thermoelastic wave to travel the length of the crystal.
- Experiment
- MD
- 13
- 

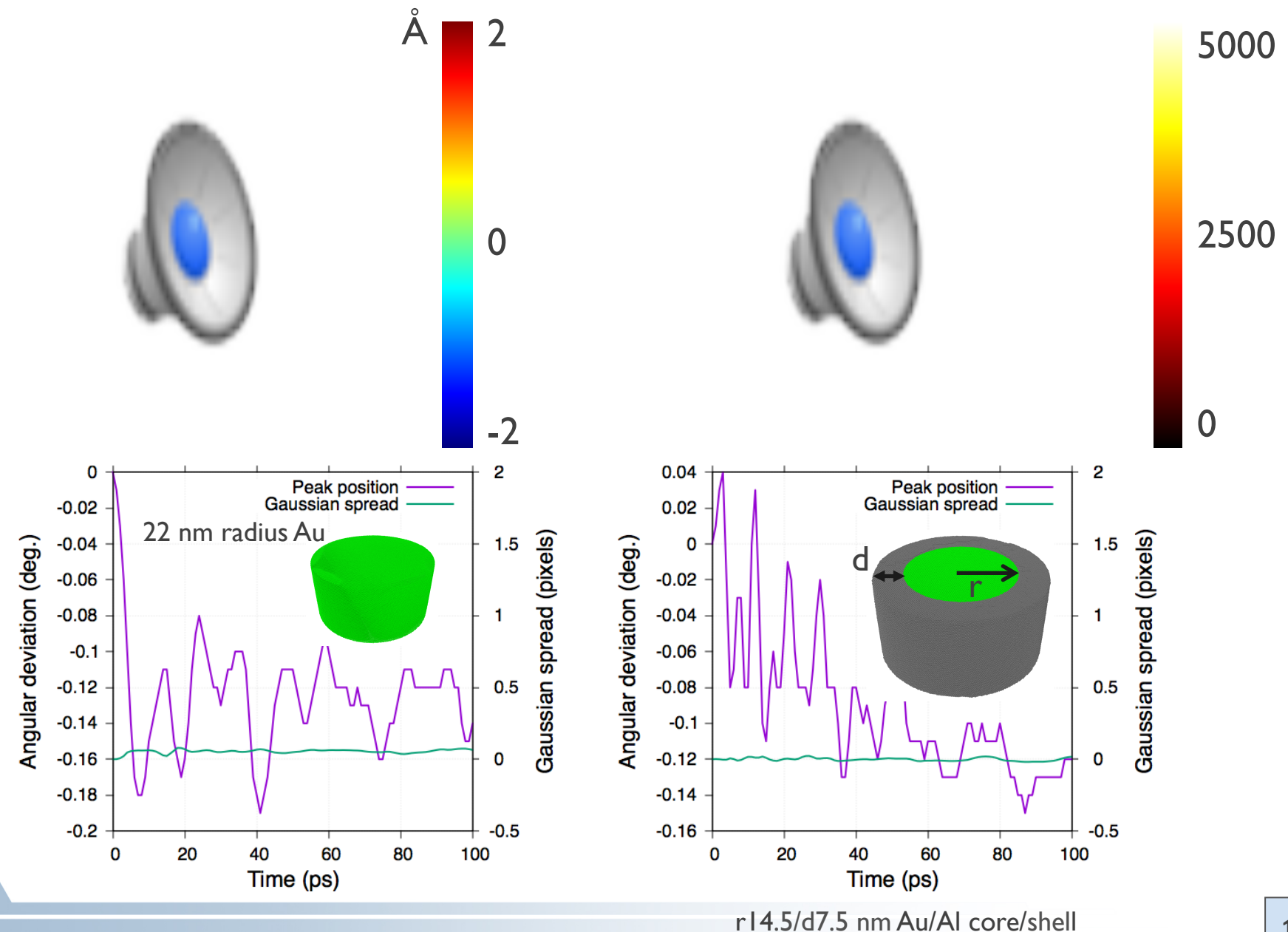


Breathing in core-shell bimetallic nanocrystals: Experiment

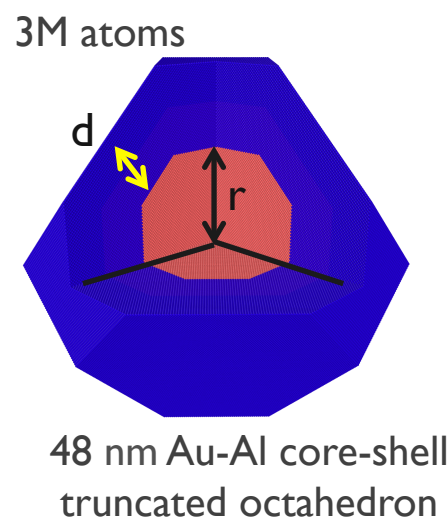
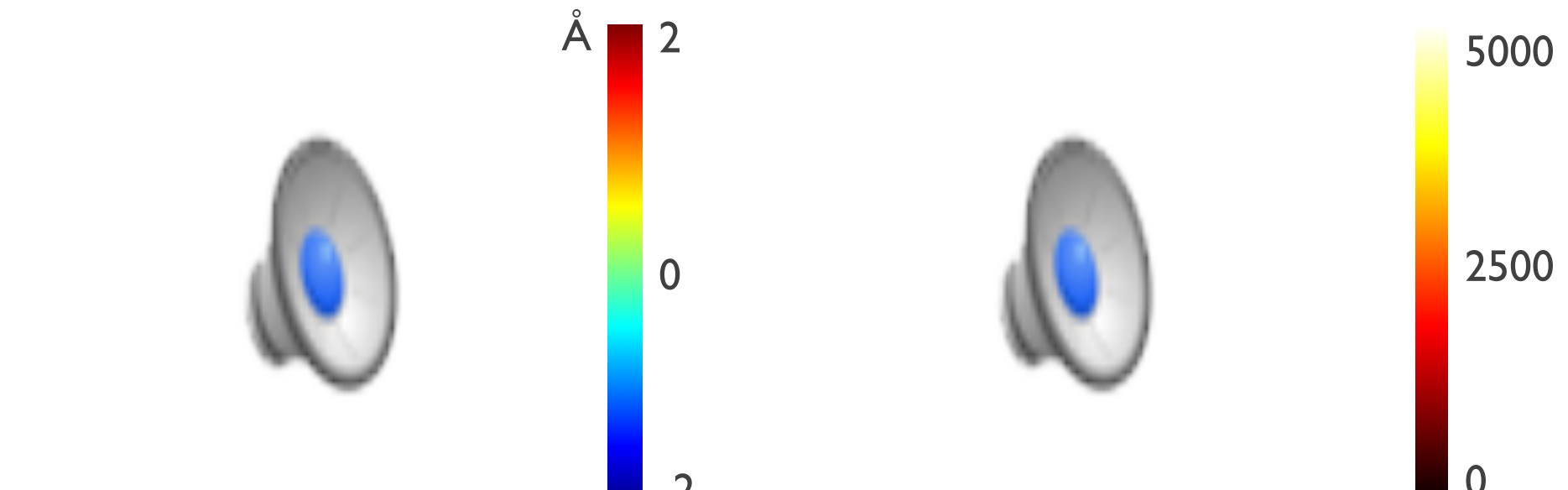


Experiments by J. N. Clark at Stanford/SLAC.

Breathing in core-shell bimetallic nanocrystals: Simulation



Breathing in core-shell bimetallic nanocrystals: Simulation

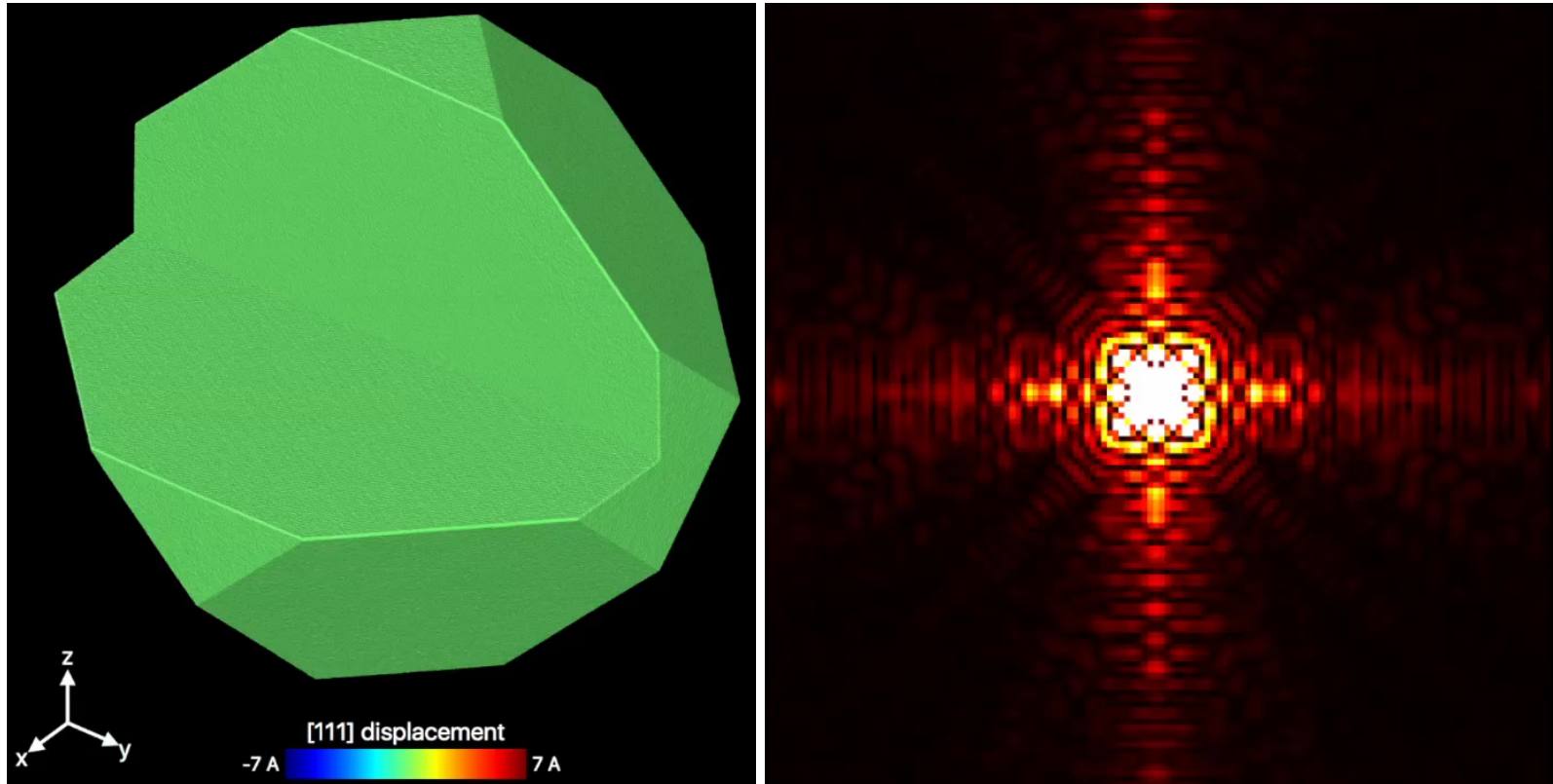


Simulation results:

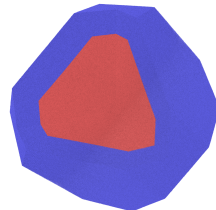
- ❖ No inhomogeneous effects observed for “small” nanocrystal sizes.
- ❖ The diffraction pattern spreading is not solely an effect of shape.



Breathing in core-shell bimetallic nanocrystals: Simulation



MD simulations → Calculated diffraction pattern

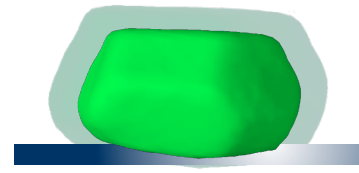


20M atoms
90 nm Au/Al core/shell truncated octahedron

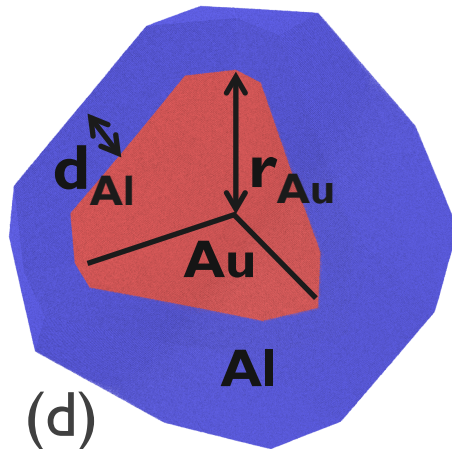
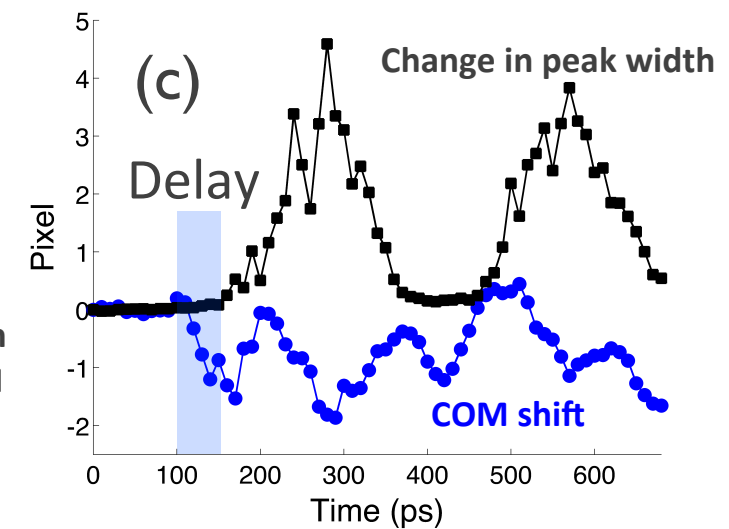
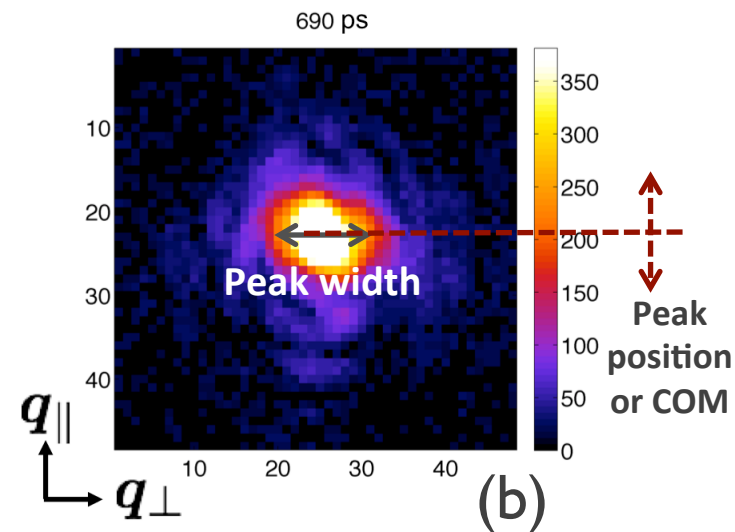


Breathing in core-shell bimetallic nanocrystals: Simulation

100 nm aluminum shell on 300 nm gold

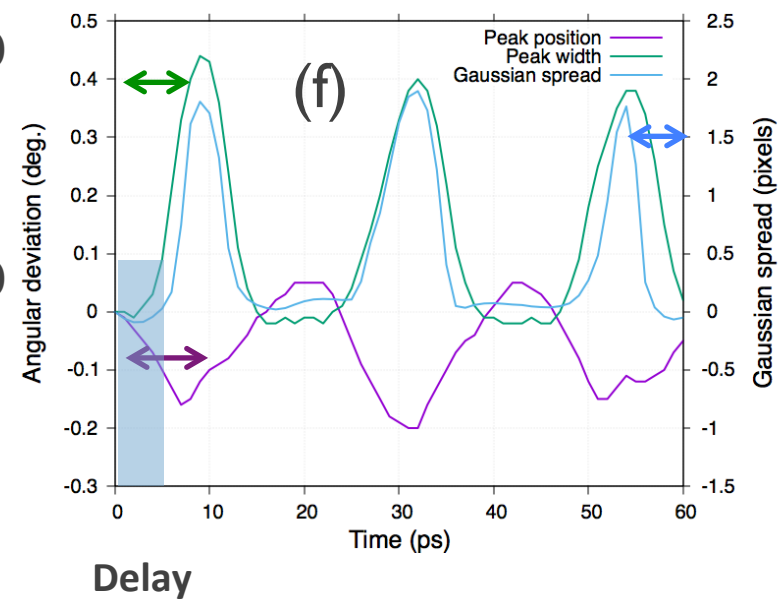
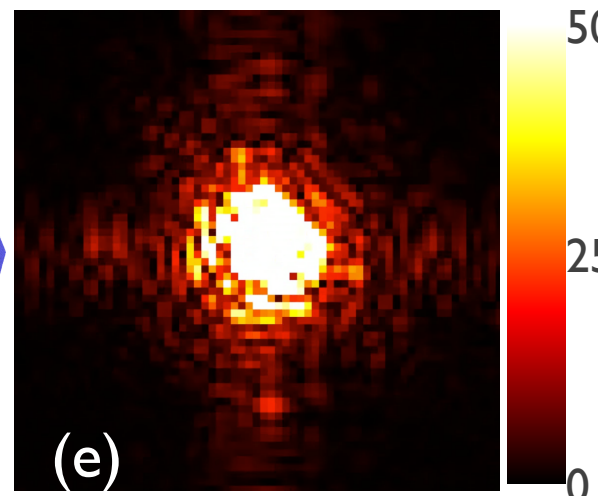


(a)

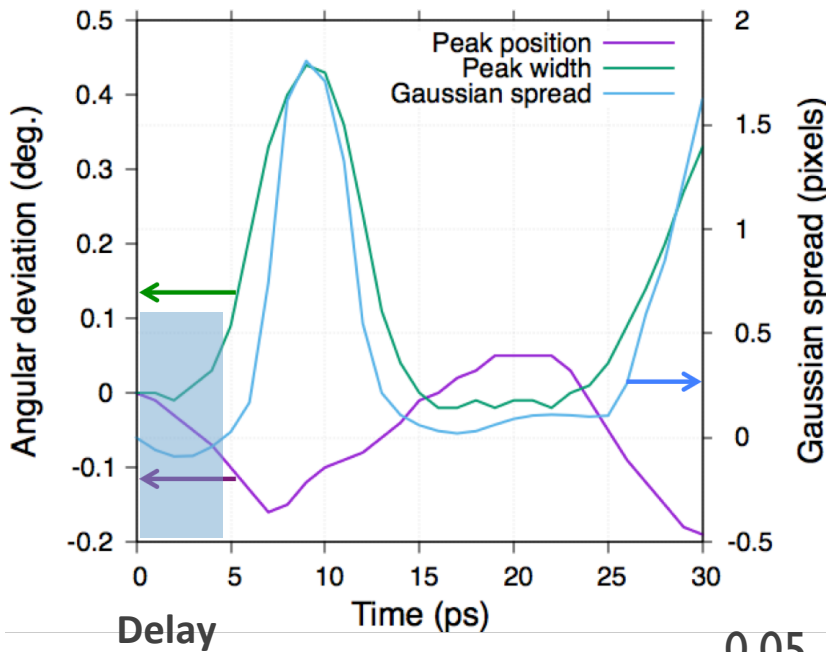


90 nm Au-Al core-shell truncated octahedron

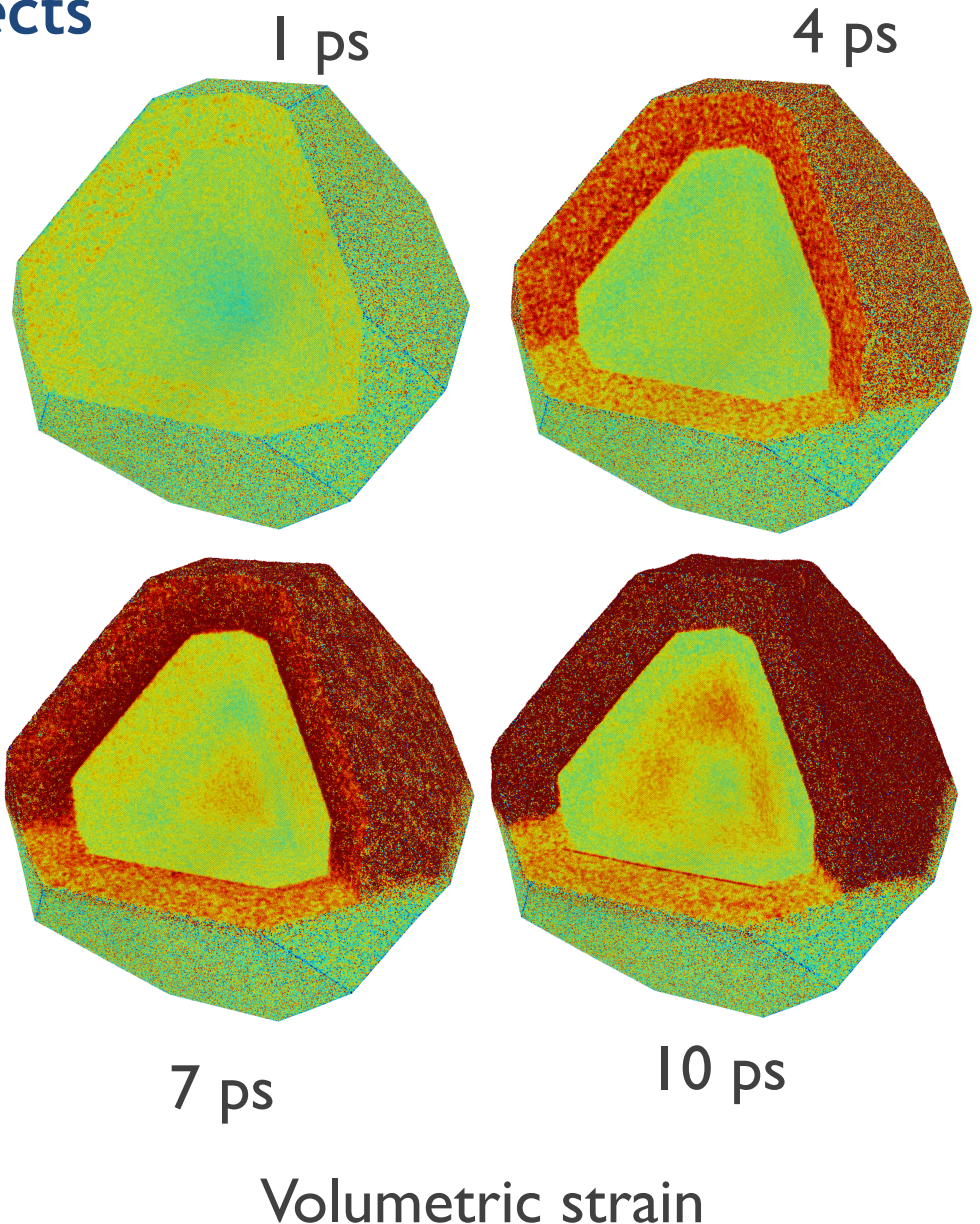
$$d_{Al}/r_{Au} = 0.3$$



Origin of inhomogeneous effects



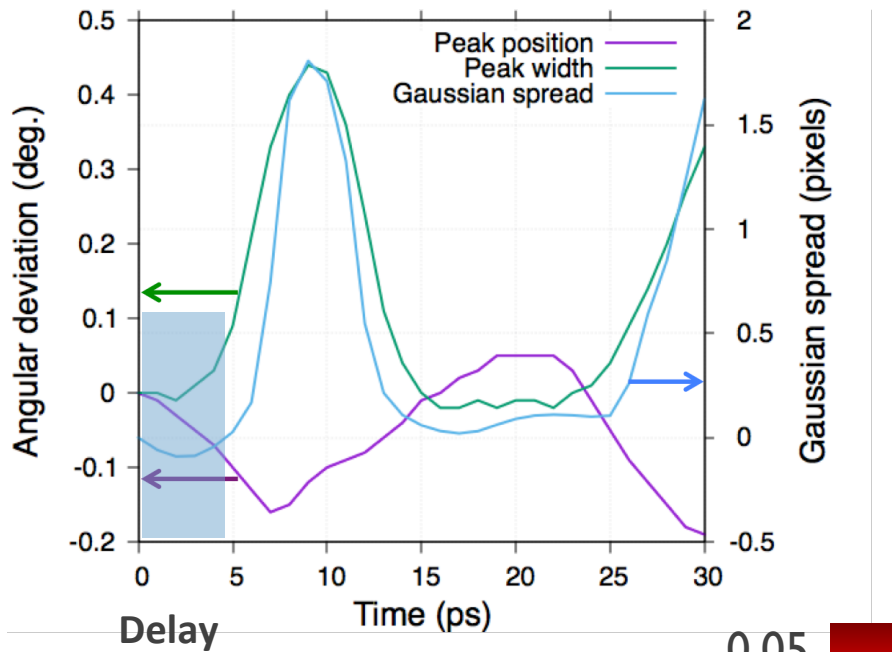
- ❖ Generation of thermoelastic wave from interface.
- ❖ 1-4 ps: No shear modes. Average lattice constant increases as gold heats up.
- ❖ Between 4 and 5 ps – reflection of thermoelastic wave and **formation of shear bands**.



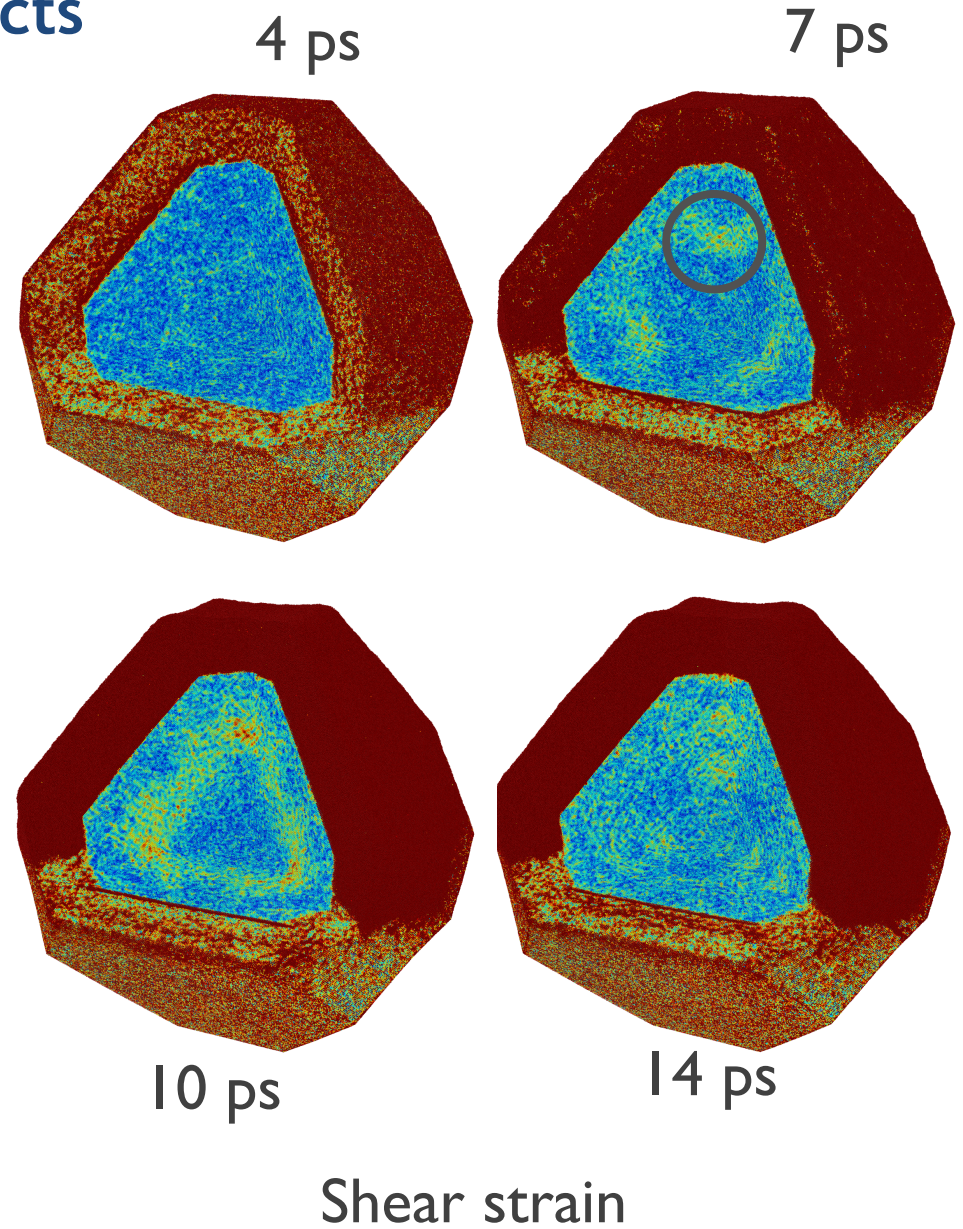
Volumetric strain



Origin of inhomogeneous effects



- ❖ Formation of shear bands is the origin of the observed inhomogeneous effects.
- ❖ Direct BCDI measurement of shear strains possible.



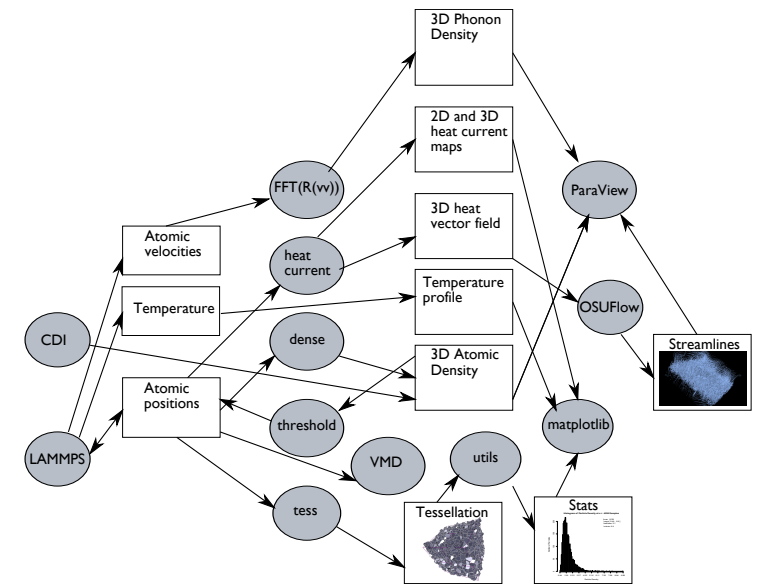
Conclusion

- ✧ Developing an automated workflow to integrate BCDI measurements with large-scale molecular dynamics simulations.
 - Gain atomistic level insight from BCDI measurements. Made possible by converging time and length scales.
 - Potential future application: Atomistically informed machine learned models to investigate corrosion using BCDI.
- ✧ Inhomogeneous deformation in core/shell nanocrystals can be measured using BCDI by investigating the shear modes.
- ✧ The shear deformation likely due to core-shell mismatch
 - Mismatch in breathing frequencies.
 - Mismatch in thermal expansion.
- ✧ The onset of shear bands depends on the core size.
- ✧ The exact size and shape of the measured diffraction pattern spreading depends on the shape of the interface.



Additional slides: MAUI workflow

- ❖ **Modeling:** Molecular Dynamics will be used to model the lattice dynamics and phonon transport.
- ❖ **Analysis:** In order to combine the reverse (image reconstruction) with the forward (simulation) models, data transformations between model spaces will be investigated.
- ❖ **Ultrafast imaging:** Laser pump-probe imaging experiments to study the structure dynamics originating from electron-phonon interactions.



Detailed workflow and tools
essential to MAUI

Integrating imaging and simulation

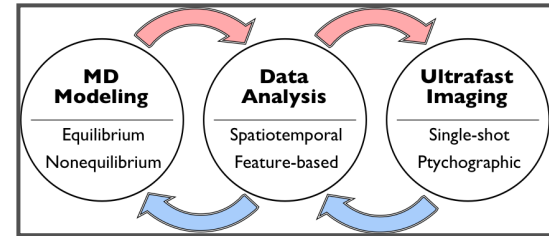
- ❖ Experimental and simulation time and length scales are rapidly converging with technological advancements.
- ❖ Two kinds of projects are considered part of MAUI.
 - Direct comparisons between experiment and theory.
 - Simulations complement experiments.



Additional slides: What is MAUI?

Goal

Integrated Imaging, Modeling, and Analysis of Ultrafast Energy Transport in Nanomaterials.



Simulation and experiment are integrated through a common language of data analysis.

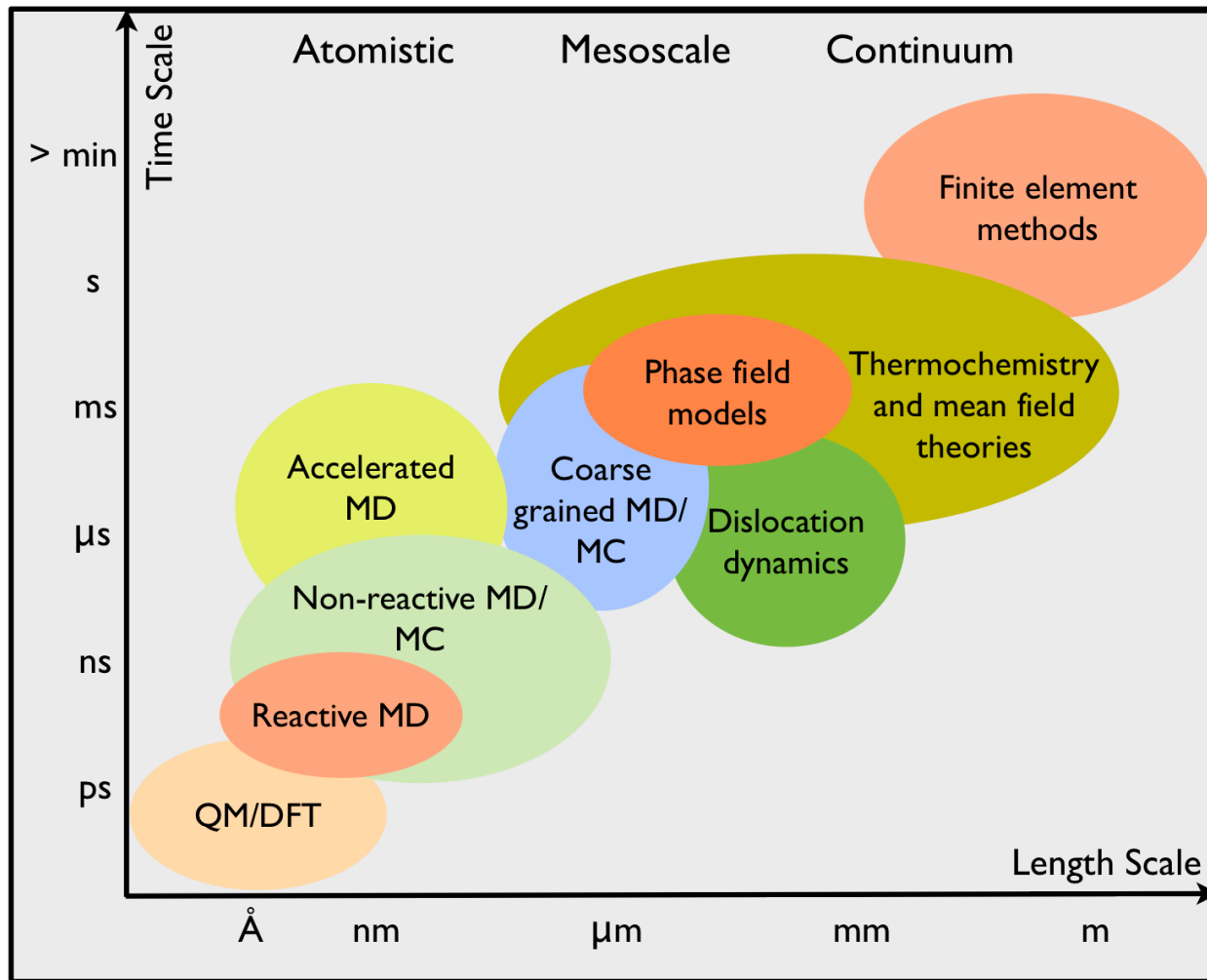
Significance and Impact

Understanding lattice vibrations in individual nanoparticles can enable several energy applications.

- ❖ Photocatalysis ❖ Semiconductor design
- ❖ Photonics ❖ Groundwater photo remediation
- ❖ Thermoelectrics ❖ Heat transfer in battery interfaces.



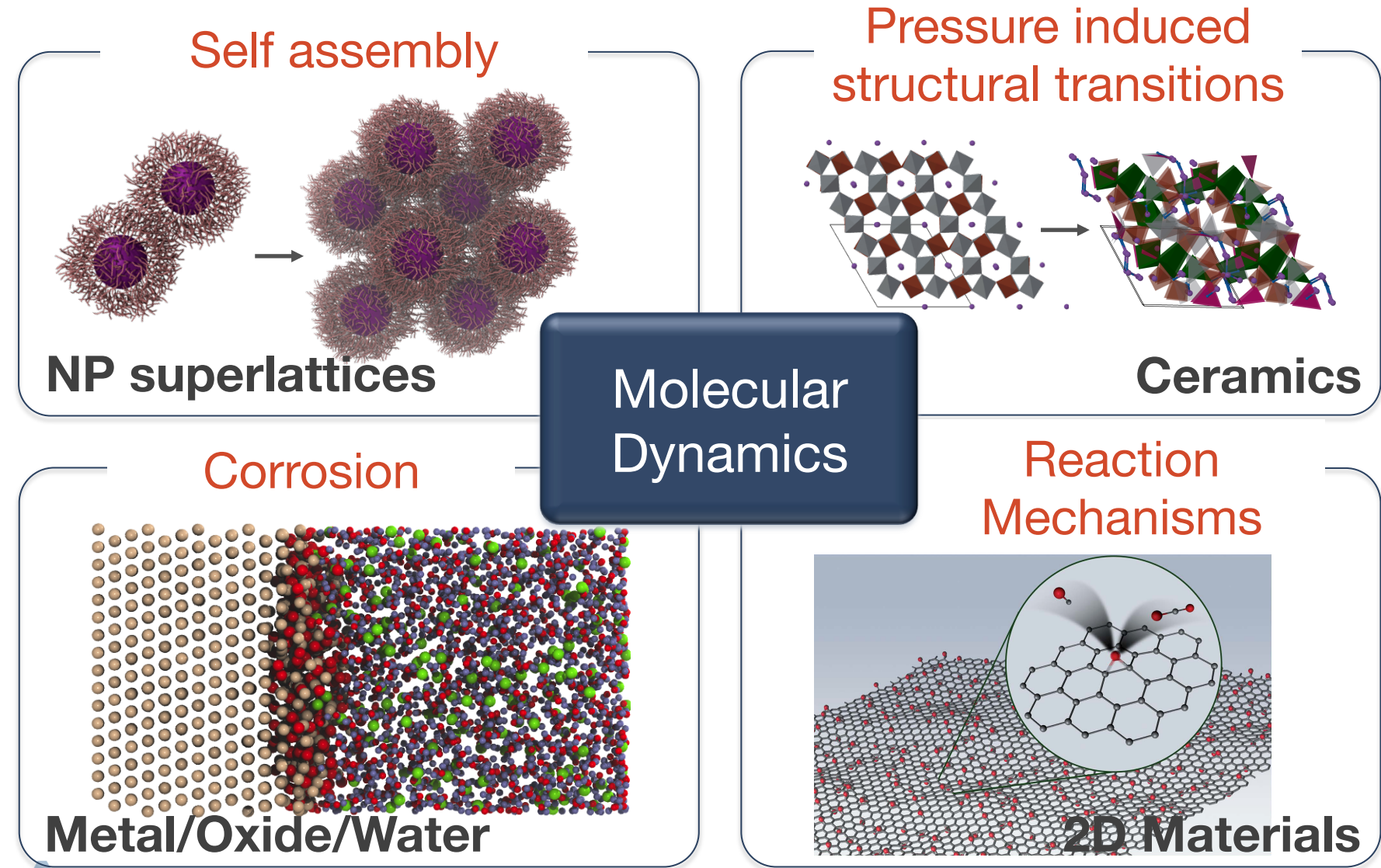
Additional slides: Molecular dynamics - accessible length and time scales



- ❖ With dedicated HPC systems classical molecular dynamics (MD) for micron length and time scales possible.
- ❖ For several interfacial phenomena, nanoscale regime required for significant deviations from bulk behavior.
- ❖ Classical and reactive MD offer powerful tools to investigate underlying physics and reaction kinetics.
 - ❖ No assumptions like mesoscale or continuum models.
 - ❖ Faster than DFT.



Additional slides: Molecular dynamics is an ideal technique to gain atomistic insights into materials phenomena

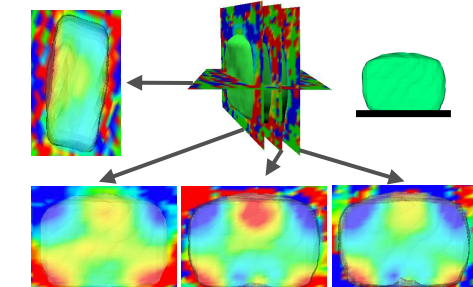


Courtesy: Badri Narayanan, ANL

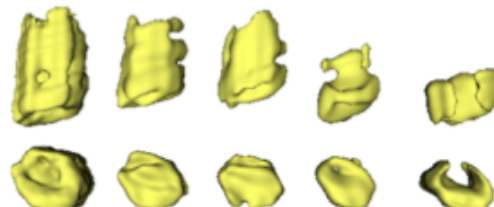
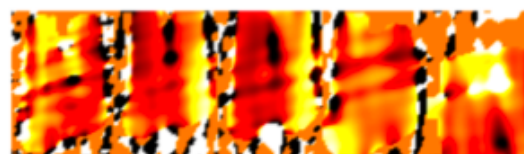
Additional slides: Coherent Diffraction Imaging Applications

In-situ and operando characterization of materials evolution

- Mechanical response at nanometer length scales
 - Structural response to chemical reactions & in-situ catalysis
 - Decomposition of semiconductors in contact with noble metals
 - Structural changes in crystals due to defect formation and removal
 - Alloying and dealloying
 - High temperature and pressure
- Domain wall (magnetic, orbital, charge) structure in the complex oxides and multi-layer
- Phase transitions vs temperature and magnetic field



Cha, Wonsuk, et. al 2013
Nat Mater 12 (8) 729–34.



Coherent diffractive imaging of solid state reactions in zinc oxide crystals.
Leake, S. J., Harder, R., & Robinson, I. K.
(2011) *New Journal of Physics*, 13(11), 113009

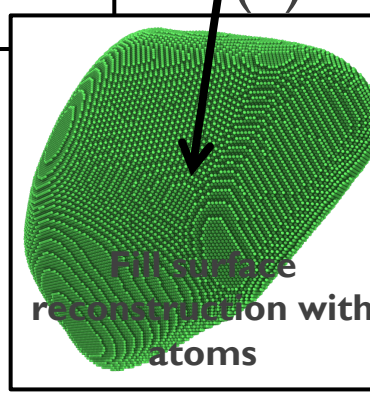
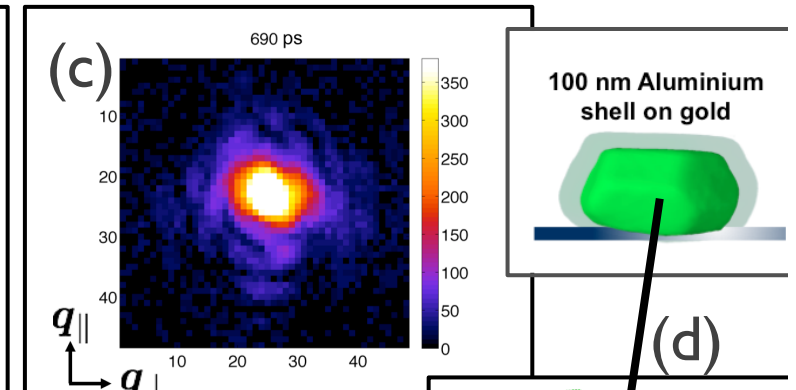
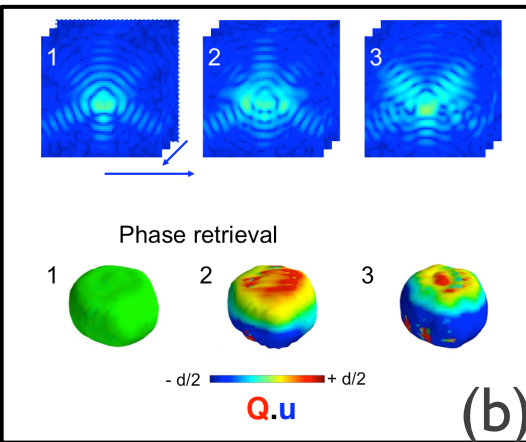
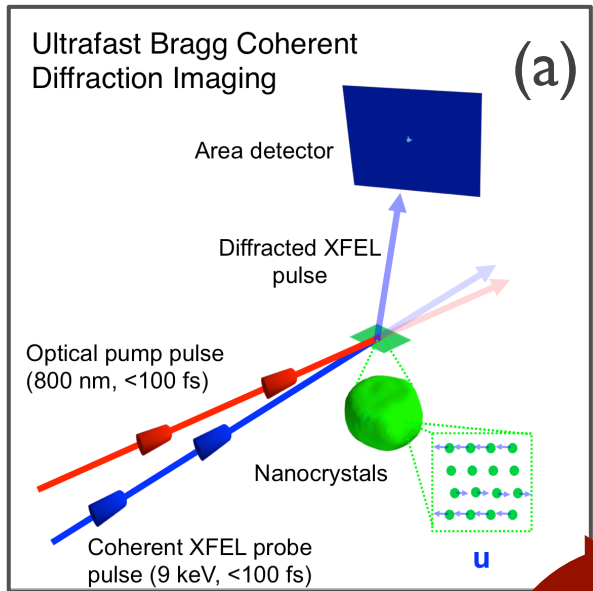
Watari, M., Harder R., et al. (2011).
Nat Mater, 10(11), 862–866.

chain thiols, the large stress cannot arise from the van der Waals interactions or other weak forces alone, but at least ionic or covalent rearrangements. Indeed the Au-S plays a crucial role in SAM formation: the structure of 1.6 nm thiolated nanocrystals has its Au-Au spaces disrupted and sulphur intermixed with gold in the outer shell. Our findings support this model and show strong lateral deformations of our 300 nm crystals with strains greater than 20 nm from the outer surface towards the crystal core. Strains are absent. The tight-radius spherical parts of nanocrystals might also undergo strong Au-S interdiffusion. We would indeed be able to provide sufficient stress for reactions involving atomic diffusion of Au at room temperature. This would also be an attractive explanation of the relatively small stress seen in both our X-ray and the cantilever experiments.

Our observation of relative contraction of the outer shell and expansion of the curved surface regions of Au nanocrystals, illustrated in Fig. 3e, leads to the conclusion that the

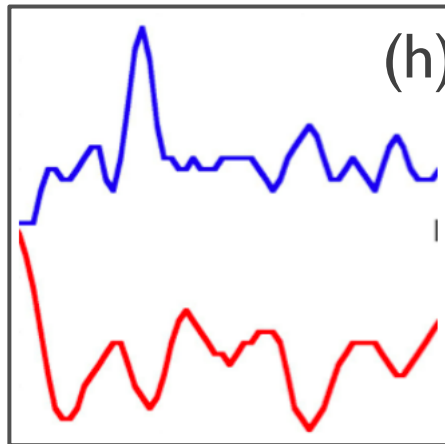
NATURE MATERIALS | VOL 10 | NOVEMBER 2011 | www.nature.com/nmat/
© 2011 Nature Publishing Group



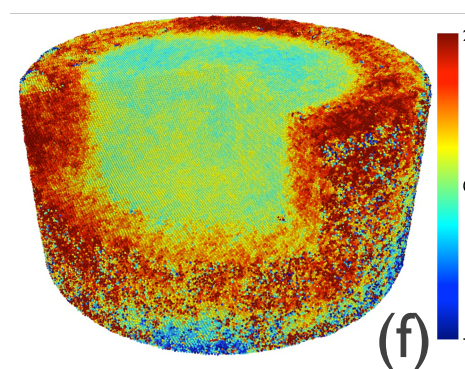
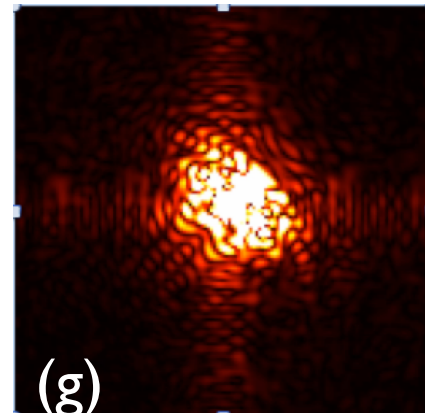


Integrated ultrafast imaging and simulation

Diffraction pattern peak position and width

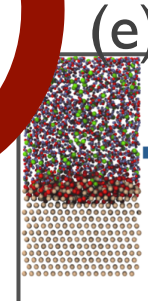


Sample diffraction pattern from molecular dynamics



Simulation via molecular dynamics

Atom positions and displacements used to compute diffraction pattern.



$$-\frac{\partial V}{\partial r_i} = m_i \frac{\partial^2 r_i}{\partial t^2}$$

$V = f(r_i)$ Force-field Interatomic potential